High Explosive Ignition through Chemically Activated Nanoscale Shear Bands

Matthew P. Kroonblawd[*] and Laurence E. Fried

Physical and Life Sciences Directorate, Lawrence Livermore National Laboratory, Livermore, California 94550, USA

Shock initiation and detonation of high explosives is considered to be controlled through hot spots, which are local regions of elevated temperature that accelerate chemical reactions. Using classical molecular dynamics, we predict the formation of nanoscale shear bands through plastic failure in shocked 1,3,5-triamino-2,4,6-trinitrobenzene high explosive crystal. By scale bridging with quantum-based molecular dynamics, we show that shear bands exhibit lower reaction barriers. While shear bands quickly cool, they remain chemically activated and support increased reaction rates without the local heating typically evoked by the hot spot paradigm. We describe this phenomenon as chemical activation through shear banding.

Preexisting microstructural heterogeneities such as voids, grain boundaries, and cracks are thought to serve as sites that can interact with a shock wave in a high explosive to produce hot spots [1]. Hot spot formation is widely regarded as the critical first step in shock initiation— the buildup to detonation from a subdetonative shock— and for sustaining a steady detonation in solid explosives [2,3]. The temperature within a hot spot greatly exceeds that in the shock-compressed bulk surroundings, thus accelerating the exothermic reaction rates and leading to possible detonation [4–6]. Despite considerable effort across decades of research, there is still uncertainty regarding the microscopic mechanisms of hot spot formation that govern the shock initiation and detonation of solid explosives.

Highly insensitive explosives offer greatly enhanced safety properties over more conventional explosives, but the physical properties responsible for the safety characteristics are not clear. 1,3,5-triamino-2,4,6-trinitrobenzene (TATB) is a highly insensitive explosive that is nearly unique in its safety-energy trade-offs. TATB is a crystalline material whose structure comprises planar layers of nearly planar TATB molecules that form a highly resilient 2D hydrogen bonding network [7–10], leading to anisotropy in its mechanical [11–13] and thermal [14,15] properties.

Continuum models for shock initiation safety and detonation performance in explosives that center on the concept of coupling between a shock wave and preexisting microstructural void defects have so far been unfruitful [3] for nonideal explosives such as TATB, which points to key physics being omitted from the model description. Several empirical continuum models do not explicitly resolve hot spots because of their small spatial scales and instead rely on empirical forms that capture the consequences of hot spot formation and evolution [3,16–18]. Some of these models require separate parameter sets for shock initiation

and detonation [16,19] or switching functions between these regimes [18], again indicating missing physics.

It is commonly held that the dominant hot spot mechanism in explosives is void collapse, which has made it the focus of the vast majority of atomistic and mesoscale studies that explicitly resolve hot spot formation (see, for instance, Refs. [6,20–26]). Shearing forces could lead to an alternative homogeneous hot spot mechanism in which they form dynamically through plastic relaxation for shock strengths above the Hugoniot elastic limit. The term "shear band" has been applied to describe both plastic relaxation resulting from activation of dislocation slip systems [27–30] and material amorphization, melting, or "shear failure" [20,31–34]. Since at least the 1970s, micron-scale shear bands have been considered as a possible route to generate heat to initiate conventional inorganic [31] and organic [32] explosives. Steric hindrance preventing dislocation slip has been proposed as driver for the increased initiation sensitivity of pentaerythritol-tetranitrate (PETN) single crystals when shocked along particular directions [30,34–37], although this concept has had limited success in explaining the initiation behavior of other explosives [27]. Grain-scale $(1–100\,\mu m)$ crystal plasticity simulations show evidence for hot lamellar shear banding structures that form dynamically in PETN single crystals following shock and could plausibly serve as a homogenous source for hot spots [29]. While shear bands are predicted and observed to form under shock loading in both organic and inorganic explosives, the chemical significance of their formation has not been well studied.

Here we develop a general multiscale modeling framework to directly probe the connections between dynamically formed shear bands and their ensuing chemistry to gain new insights into the shock initiation and detonation of explosives. Using this framework, we uncover a nanoscale shear banding mechanism that activates chemistry in TATB

through a reduction in reaction barriers. All-atom molecular dynamics (MD) simulations offer a practical route to determine parameters and elucidate guiding physical forms for continuum-scale models and are an integral component of a physics-based multiscale explosives modeling framework [24,26,38,39]. Simulations involving millions of atoms are typically required to explicitly resolve the propagation of a shock front and the evolution of crystal deformation and heat localization, which all but necessitates use of a classical force field [33,40,41]. This is in contrast to steady-state shock simulation methods [42–48], which are ill suited to study shear band formation since they do not resolve the shock front. At the same time, computationally expensive quantum-mechanical methods such as density functional theory (DFT) [49,50] are the standard for accurate quantum-based MD (QMD) predictions of chemistry. The extreme computational expense of DFT-based QMD typically limits studies to a few hundred atoms with trajectories that are a few 10s of ps in length. Highly efficient semiempirical density functional tight-binding (DFTB) [51–54] offers a competitive balance between computational efficiency and accuracy for QMD simulations of sub-ns chemistry in shocked organic systems and is a nearly optimal choice for insensitive and slow-to-react explosives, including TATB [45,47,55–58].

We develop and employ a scale bridging strategy using nonreactive classical MD and ensembles of efficient DFTB-based QMD simulations to accurately treat both the initial mechanics of TATB single crystal plasticity during shock and the ensuing sub-ns chemistry. This has a decided advantage in that we treat both the mechanics and chemistry with the best available and highest fidelity techniques that can be practically applied to model these processes. Using classical MD, we uncover a shear banding mechanism that manifests in oriented TATB crystals shocked to the steady detonation pressure ($\approx$30 GPa) and results in substantial local heating and amorphization. Chemical kinetics determined from QMD simulations reveal that TATB in shear bands is highly reactive and that shear banding is a plausible ignition mechanism that activates during steady detonation in TATB-based explosives. Our results demonstrate that shear band ignition arises on the nanoscale through coupling between crystal mechanics and chemistry that is decidedly more complex than simple localization of heat.

Molecular dynamics simulations were performed using the LAMMPS code [59] and 3D periodic simulation cells. The generalized crystal-cutting method (GCCM) [60] was used to construct a large triclinic simulation cell, shown in Fig. 1, that contained oriented TATB single crystal in the ambient $P\bar{1}$ phase [7] for classical MD shock simulations in a reverse ballistic configuration [40]. Studying the response of a perfect single crystal provides a meaningful lower bound on the shear band concentration relative to real defective TATB crystals [61] and could also provide a baseline for
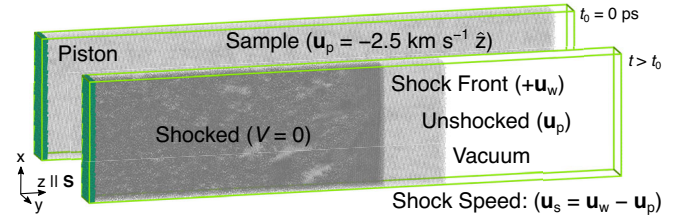

FIG. 1. Reverse ballistic simulation cell wherein a flexible sample is assigned velocity $\mathbf{u_p}$ and impacted onto a rigid piston, generating a shock wave that travels at velocity $\mathbf{u_w}$ with respect to the piston and at velocity $\mathbf{u_s} = \mathbf{u_w} - \mathbf{u_p}$ through the sample. Material velocity V behind the front goes to zero.

comparison to future experiments using new high quality single crystals [10]. The shock direction **S** was oriented along z in the lab frame and was set to be 15° away from the normal to the TATB crystal layers $\mathbf{N}_{(001)}$ in the plane defined by lattice vector **a** and $\mathbf{N}_{(001)}$. The (x, y, z) crystal dimensions were (61.4 nm, 7.9 nm, 260.8 nm) with all cell angles within 0.4° of 90°, which corresponds to 13.3 million atoms. All simulation snapshots were prepared with OVITO [62].

Classical MD simulations were performed using a well-established nonreactive force field for TATB [11,14,63]. See Supplemental Material [64] for descriptions of the MD algorithms used [65–72]. We chose $\mathbf{u_p} = -2.5$ km s^{-1} to generate an $\approx$30 GPa shock, which is close to the von Neumann shock pressure (estimated to be 34 GPa [19]) in TATB. The material response was characterized through locally averaged molecular quantities, including the temperature, shear stress, and an order parameter that differentiates between bulk and shear band configurations. The temperature T was obtained through the molecular roto-librational and vibrational kinetic energy. To account for the well-known error in the heat capacity of classical systems, we obtained quantum-corrected molecular temperatures through a temperature-dependent molecular specific heat. That is, we solved

$$\Delta E_{\text{ro-vib}} = \int_{300 \text{ K}}^{T} [3k_B + C_V(T')] dT', \qquad (1)$$

for the upper integration limit, where $\Delta E_{\text{ro-vib}}$ is twice the change in ro-vibrational kinetic energy relative to the preshock state and the molecular specific heat under the integral is separated into a classical contribution from the roto-librations ($3k_B$) and a quantum-mechanical contribution $C_V(T)$ from the molecular vibrations obtained from a DFT-based quasi-harmonic prediction [41]. Shear was characterized using the von Mises stress, σ_{Mises}, a rotationally invariant measure of deviatoric stress. A structural order parameter was defined using the second Legendre polynomial,

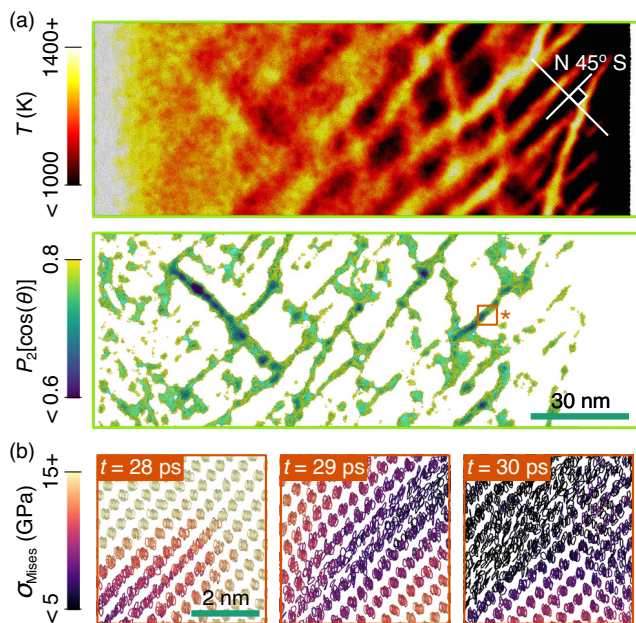$$P_2[\cos(\theta)] = \frac{1}{2}[3\cos^2(\theta) - 1], \qquad (2)$$

FIG. 2. (a) Snapshots of the simulation cell showing locally averaged molecular properties at maximum compression ($t = 38$ ps), including (top) T with projecting plane $\mathbf{N}$ for the analysis in Fig. 3, and (bottom) $P_2[\cos(\theta)]$ order parameter where crystalline molecules with $P_2[\cos(\theta)] > 0.8$ were removed and used to interpolate a bounding surface. (b) Renderings of the TATB C_6 rings in region * showing shear band growth.

FIG. 3. Average T and $P_2[\cos(\theta)]$ values at three different times projected onto a plane $\mathbf{N}$ that forms a 45° angle with respect to the shock direction $\mathbf{S}$. The averages were taken over molecules falling within 10 nm of the projecting plane and include periodically equivalent images where the plane falls outside the primary cell.

where θ is computed in terms of the TATB benzene ring unit normal vector $\mathbf{Q}(t)$ with respect to its value at the start of the simulation as $\cos(\theta) = \mathbf{Q}(t) \cdot \mathbf{Q}(0)$. A value of 0 corresponds to complete loss of the initial rotational order, while 1 corresponds to no orientational change. See Supplemental Material [64] for further simulation and analysis details.

Figure 2(a) shows the response of shocked oriented TATB single crystal at the moment of maximum compression. The most striking feature is the formation and growth of hot planar bands at ≈45° with respect to the shock direction. Comparison of T and $P_2[\cos(\theta)]$ indicates that hot shear band regions also exhibit significant loss of the original crystalline order. Figure 2(b) highlights the nm-scale growth process for a selected shear band in region *. After passage of the shock front, the material is under a very high deviatoric stress indicated by σ_{Mises}. As the shear band grows, it simultaneously relieves deviatoric stress and leads to amorphization in its wake through a ps-scale material shear failure process. Similar shear bands were predicted to form for shocks propagating along [100] in the related molecular explosive α-cyclotrimethylene-trinitr-amine (α-RDX) [33] and are akin to phenomenological mesoscale descriptions that treat shear bands as melted regions [20]. This shear failure process is distinct from dislocation-mediated shear banding seen in PETN [30] and for the $\mathbf{N}_{(111)}$ [27] and $\mathbf{N}_{(021)}$ [28] directions in α-RDX.
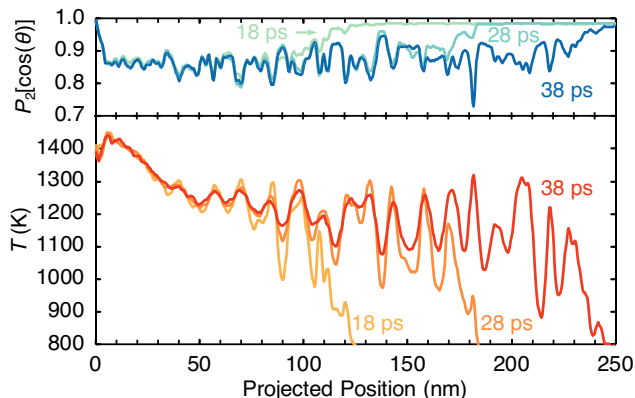
Material in the shear band regions is 5.5% denser than the surrounding crystal. The shear bands do not fully liquify, and the shear band temperature and pressure state is below the predicted melting point for TATB [63,73]. More detailed characterizations of the density, local deformation, and temperature field of shear bands are given in the Supplemental Material [64].

We projected the average molecular T and $P_2[\cos(\theta)]$ values onto a plane that is orthogonal to the direction of shear band growth to assess the shear band dimensions, temperature, and structure (see Fig. 3). Most of the bands are roughly 10 nm wide and reach an average temperature of 1300 K. Comparing the temperature curves at $t = 38$ ps to those at earlier times reveals relaxation occurring in roughly 20 ps through thermal conduction, with an approximate average (and thus final) temperature being near 1200 K. Regions with the highest temperatures coincide with the lowest average orientational order. Regions between the bands exhibit near crystalline $P_2[\cos(\theta)]$ values and are also initially cooler (≈1000 K). Shear bands also developed in simulation cells with smaller transverse dimensions (see Supplemental Material [64]).

Representative shocked bulk crystalline and shear band configurations were extracted from our large-scale classical MD simulation for DFTB-based chemistry studies and are shown in Fig. 4. Each cell was 3D periodic and contained eight molecules (192 atoms) of unreacted TATB at the average postshock density 2.96 g cm^{-3}. A chemical kinetics study was performed using ensembles of iso-thermal-isochoric (NVT) QMD simulations driven by DFTB+ [74]. Ten simulations were performed per configuration type and per temperature in 200 K increments in the interval 2400 K ≤ T ≤ 3200 K. A graph-based analysis of interatomic bonding determined through a distance and
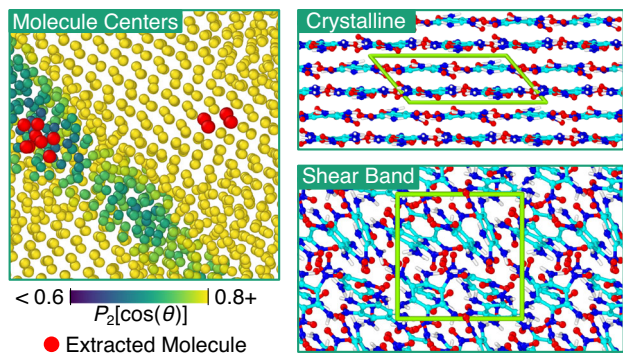
FIG. 4. Representative shock-compressed bulk crystalline and shear band configurations extracted from the vicinity of the shear band for QMD simulations. Atoms are colored cyan, blue, red, and white for C, N, O, and H, the primary QMD simulation cell is drawn in light green, and truncated replications of that cell are shown to highlight the packing structure.
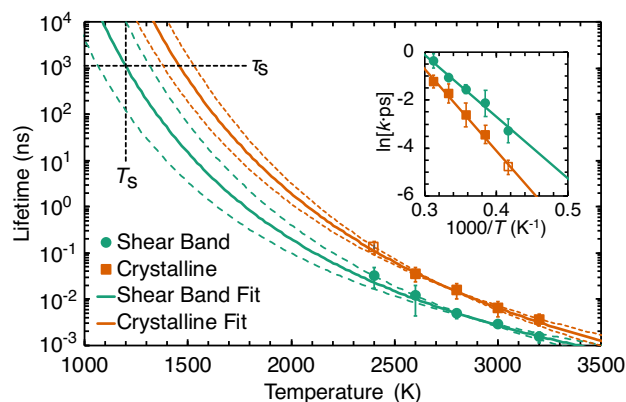

FIG. 5. Predicted lifetimes for TATB in crystalline and shear band regions obtained from NVT QMD simulations and Arrhenius fits to the QMD results. Solid curves correspond to fitted values and dashed curves to a 1σ uncertainty estimate. The inset plots the same data in terms of the ln of the reaction rate k versus $1000/T$. Each data point corresponds to the average of ten independent QMD simulations and error bars to 1σ. The crystal data point at 2400 K is shown with an open symbol as only nine simulations reacted within 200 ps. The equilibrium temperature and reaction lifetime for the shear bands are indicated by T_s and τ_s, respectively.

lifetime criterion was performed to characterize the chemistry. The characteristic reaction time was defined as the time required for half of the TATB C_6 rings to dissociate, as identified by a cycle analysis using NETWORKX [75]. Each trajectory was integrated past its characteristic time, up to a maximum of 200 ps. Additional QMD simulations described in the Supplemental Material [64] show that the predicted kinetics are insensitive to both the density variations and the small cell size.

Results from our ensembles of QMD simulations are shown in Fig. 5 along with weighted fits of the rates k to an Arrhenius expression, $k = A\exp(-E_a/RT)$. The average characteristic times for bulk crystalline and shear band TATB are clearly different within uncertainty at each temperature considered, with the shear band configurations reacting much more quickly. Weighted Arrhenius fits indicate that shear band configurations exhibit a significant reduction in activation energy E_a relative to crystalline configurations. These activation energies are respectively 51 ± 9 kcal mol^{-1} and 68 ± 7 kcal mol^{-1}. A more detailed reaction analysis shows that TATB in shear bands is more likely to emit NO_2 groups as an initial step, which accelerates the decomposition. At the same time, shear bands exhibit a lower population of species associated with intra- and intermolecular hydrogen transfers that initiate chemistry in the crystal [45,47]. This indicates that shear band configurations exhibit a mechanochemical influence on the kinetics [76,77] that may favor alternative reaction channels. Additional details are given in the Supplemental Material [64].

The maximum shear band temperature in Fig. 2 is 1300 K. According to Fig. 5, the reaction time at this temperature is 200 ns in the shear band regions. This is much longer than the 20 ps time for thermal relaxation of the shear band. Therefore, the approximate equilibrium temperature ($T_s \approx 1200$ K) is most relevant to thermally activated chemistry. At T_s, reactions are predicted to occur

in the shear bands within ≈ 1 μs, which is 2 orders of magnitude faster than for the crystalline bulk (≈ 180 μs). The predicted lifetimes are larger than the TATB reaction zone time (≈ 100–300 ns [19]). Our previous experience with applying standard DFTB parameter sets to organic systems indicates that reaction barriers are systematically overestimated by 5–10 kcal mol^{-1} [78,79]. Accounting for this systematic bias translates to an average lifetime of ≈ 14 ns for TATB in shear bands and a lower bound of 0.3 ns when coupled with our quantified random uncertainties, indicating that shear bands in TATB could plausibly ignite during the reported reaction zone time. While the present results consider shear bands in isolation, they could also form and couple with other hot spot sources to enhance local reaction rates during shock initiation. Preliminary simulations show shear band formation at pressures between 8 and 30 GPa, which corresponds to the measured region of shock initiation.

Following ignition of material in a shear band, a high-pressure deflagration process is expected to consume the rest of the explosive material. This mechanism has been referred to as reaction growth in models such as Lee and Tarver's Ignition and Growth model [16]. We can estimate the rate of reaction growth in a shear band by assuming a steady laminar premixed burn. Combustion theory indicates that the laminar burn velocity is proportional to the square root of the reaction rate at the burning temperature, while other terms depend on properties of the burned products that are likely to be nearly the same in shear bands and the bulk [80,81]. Using 2360 K as a calculated [82] burning temperature for TATB (see Supplemental Material

[64]), we estimate that laminar burn rates will be 2.2 times greater in the shear bands than in the bulk.

Our scale bridging approach overcomes the prohibitive computational expense of quantum-based MD applied to large systems and treats both crystal mechanics and chemistry with the best available models for the relevant time and length scales. We show that highly reactive nanoscale shear bands are formed in TATB shocked near its von Neumann pressure. We demonstrate that shear banding in explosives can lead to ignition *via* chemical activation through shear banding—a process that hinges on the reduction in activation energy. This is distinct from the traditional hot spot concept, where local heating is the dominant mechanism that leads to increased chemical reaction rate. Inclusion of shear band formation into continuum shock initiation models [83] in the future could lead to significant improvements in safety and performance assessments. Given many prior results regarding shear band formation in shocked explosives, we believe that this mechanism could be important in a wide range of energetic materials.

---

*Corresponding author.
 kroonblawd1@llnl.gov

[1] J. E. Field, Acc. Chem. Res. **25**, 489 (1992).
[2] R. Menikoff, AIP Conf. Proc. **1195**, 18 (2009).
[3] C. A. Handley, B. D. Lambourn, N. J. Whitworth, H. R. James, and W. J. Belfield, Appl. Phys. Rev. **5**, 011303 (2018).
[4] C. L. Mader, Phys. Fluids **8**, 1811 (1965).
[5] B. L. Holian, T. C. Germann, J.-B. Maillet, and C. T. White, Phys. Rev. Lett. **89**, 285501 (2002).
[6] M. A. Wood, M. J. Cherukara, E. M. Kober, and A. Strachan, J. Phys. Chem. C **119**, 22008 (2015).
[7] H. H. Cady and A. C. Larson, Acta Crystallogr. **18**, 485 (1965).
[8] A. J. Davidson, R. P. Dias, D. M. Dattelbaum, and C.-S. Yoo, J. Chem. Phys. **135**, 174507 (2011).
[9] M. R. Manaa and L. E. Fried, J. Phys. Chem. C **116**, 2116 (2012).
[10] B. A. Steele, S. M. Clarke, M. P. Kroonblawd, I.-F. W. Kuo, P. F. Pagoria, S. N. Tkachev, J. S. Smith, S. Bastea, L. E. Fried, J. M. Zaug, E. Stavrou, and O. Tschauner, Appl. Phys. Lett. **114**, 191901 (2019).
[11] D. Bedrov, O. Borodin, G. D. Smith, T. D. Sewell, D. M. Dattelbaum, and L. L. Stevens, J. Chem. Phys. **131**, 224703 (2009).
[12] N. Mathew and T. D. Sewell, J. Phys. Chem. C **120**, 8266 (2016).
[13] P. Lafourcade, C. Denoual, and J.-B. Maillet, J. Phys. Chem. C **122**, 14954 (2018).
[14] M. P. Kroonblawd and T. D. Sewell, J. Chem. Phys. **139**, 074503 (2013).
[15] M. P. Kroonblawd and T. D. Sewell, J. Phys. Chem. C **120**, 17214 (2016).
[16] E. L. Lee and C. M. Tarver, Phys. Fluids **23**, 2362 (1980).
[17] J. N. Johnson, P. K. Tang, and C. A. Forest, J. Appl. Phys. **57**, 4323 (1985).
[18] B. L. Wescott, D. S. Stewart, and W. C. Davis, J. Appl. Phys. **98**, 053514 (2005).
[19] C. M. Tarver, J. W. Kury, and R. D. Breithaupt, J. Appl. Phys. **82**, 3771 (1997).
[20] R. A. Austin, N. R. Barton, J. E. Reaugh, and L. E. Fried, J. Appl. Phys. **117**, 185902 (2015).
[21] R. M. Eason and T. D. Sewell, J. Dyn. Behav. Mater. **1**, 423 (2015).
[22] G. A. Levesque and P. Vitello, Propellants Explos. Pyrotech. **40**, 303 (2015).
[23] H. K. Springer, S. Bastea, A. L. Nichols III, C. M. Tarver, and J. E. Reaugh, Propellants Explos. Pyrotech. **43**, 805 (2018).
[24] M. A. Wood, D. E. Kittell, C. D. Yarrington, and A. P. Thompson, Phys. Rev. B **97**, 014109 (2018).
[25] N. K. Rai and H. S. Udaykumar, Phys. Fluids **31**, 016103 (2019).
[26] P. Zhao, S. Lee, T. Sewell, and H. S. Udaykumar, Propellants Explos. Pyrotech. **45**, 196 (2020).
[27] M. J. Cawkwell, K. J. Ramos, D. E. Hooks, and T. D. Sewell, J. Appl. Phys. **107**, 063512 (2010).
[28] K. J. Ramos, D. E. Hooks, T. D. Sewell, and M. J. Cawkwell, J. Appl. Phys. **108**, 066105 (2010).
[29] J. J. Rimoli, E. Gürses, and M. Ortiz, Phys. Rev. B **81**, 014112 (2010).
[30] R. M. Eason and T. D. Sewell, J. Phys. Chem. C **116**, 2226 (2012).
[31] R. E. Winter, J. E. Field, and D. Tabor, Proc. R. Soc. A **343**, 399 (1975).
[32] R. B. Frey, in *Seventh Symposium (International) on Detonation* (Naval Surface Weapons Center, Dahlgren, VA, 1981), p. 36.
[33] M. J. Cawkwell, T. D. Sewell, L. Zheng, and D. L. Thompson, Phys. Rev. B **78**, 014107 (2008).
[34] M. J. Cawkwell, N. Mohan, D. J. Luscher, and K. J. Ramos, Philos. Mag. **99**, 1079 (2019).
[35] J. J. Dick, Appl. Phys. Lett. **44**, 859 (1984).
[36] J. J. Dick, R. N. Mulford, W. J. Spencer, D. R. Pettit, E. Garcia, and D. C. Shaw, J. Appl. Phys. **70**, 3572 (1991).
[37] S. V. Zybin, W. A. Goddard, P. Xu, A. C. T. van Duin, and A. P. Thompson, Appl. Phys. Lett. **96**, 081918 (2010).
[38] R. Menikoff and T. D. Sewell, Combust. Theory Modell. **6**, 103 (2002).
[39] B. C. Barnes, J. K. Brennan, E. F. C. Byrd, S. Izvekov, J. P. Larentzos, and B. M. Rice, Toward a predictive hierarchical multiscale modeling approach for energetic materials, in *Computational Approaches for Chemistry Under Extreme Conditions*, edited by N. Goldman (Springer International Publishing, Cham, 2019), p. 229.
[40] B. L. Holian and P. S. Lomdahl, Science **280**, 2085 (1998).
[41] M. P. Kroonblawd, T. D. Sewell, and J.-B. Maillet, J. Chem. Phys. **144**, 064501 (2016).
[42] J.-B. Maillet, M. Mareschal, L. Soulard, R. Ravelo, P. S. Lomdahl, T. C. Germann, and B. L. Holian, Phys. Rev. E **63**, 016121 (2000).

[43] E. J. Reed, L. E. Fried, and J. D. Joannopoulos, Phys. Rev. Lett. **90**, 235503 (2003).

[44] R. Ravelo, B. L. Holian, T. C. Germann, and P. S. Lomdahl, Phys. Rev. B **70**, 014103 (2004).

[45] M. R. Manaa, E. J. Reed, L. E. Fried, and N. Goldman, J. Am. Chem. Soc. **131**, 5483 (2009).

[46] K. Shimamura, M. Misawa, S. Ohmura, F. Shimojo, R. K. Kalia, A. Nakano, and P. Vashishta, Appl. Phys. Lett. **108**, 071901 (2016).

[47] Z.-H. He, J. Chen, and Q. Wu, J. Phys. Chem. C **121**, 8227 (2017).

[48] B. W. Hamilton, M. P. Kroonblawd, M. M. Islam, and A. Strachan, J. Phys. Chem. C **123**, 21969 (2019).

[49] P. Hohenberg and W. Kohn, Phys. Rev. **136**, B864 (1964).

[50] W. Kohn and L. J. Sham, Phys. Rev. **140**, A1133 (1965).

[51] J. C. Slater and G. F. Koster, Phys. Rev. **94**, 1498 (1954).

[52] M. Elstner, D. Porezag, G. Jungnickel, J. Elsner, M. Haugk, T. Frauenheim, S. Suhai, and G. Seifert, Phys. Rev. B **58**, 7260 (1998).

[53] M. Elstner, T. Frauenheim, E. Kaxiras, G. Seifert, and S. Suhai, Phys. Status Solidi B **217**, 357 (2000).

[54] T. Krüger, M. Elstner, P. Schiffels, and T. Frauenheim, J. Chem. Phys. **122**, 114110 (2005).

[55] E. J. Reed, M. Riad Manaa, L. E. Fried, K. R. Glaesemann, and J. D. Joannopoulos, Nat. Phys. **4**, 72 (2008).

[56] M. J. Cawkwell, A. M. N. Niklasson, and D. M. Dattelbaum, J. Chem. Phys. **142**, 064512 (2015).

[57] L. Koziol and N. Goldman, Astrophys. J. **803**, 91 (2015).

[58] M. P. Kroonblawd and N. Goldman, Phys. Rev. B **97**, 184106 (2018).

[59] S. Plimpton, J. Comput. Phys. **117**, 1 (1995); LAMMPS is available at http://lammps.sandia.gov.

[60] M. P. Kroonblawd, N. Mathew, S. Jiang, and T. D. Sewell, Comput. Phys. Commun. **207**, 232 (2016).

[61] D. M. Hoffman, T. M. Willey, A. R. Mitchell, and S. C. Depiero, J. Energy Mater. **26**, 139 (2008).

[62] A. Stukowski, Model. Simul. Mater. Sci. Eng. **18**, 015012 (2010); OVITO is available at https://www.ovito.org.

[63] N. Mathew, T. D. Sewell, and D. L. Thompson, J. Chem. Phys. **143**, 094706 (2015).

[64] See Supplemental Material at http://link.aps.org/supplemental/10.1103/PhysRevLett.124.206002 for additional simulation and analysis details.

[65] N. D. Mermin, Phys. Rev. **137**, A1441 (1965).

[66] H. C. Andersen, J. Comput. Phys. **52**, 24 (1983).

[67] S. Nosé, J. Chem. Phys. **81**, 511 (1984).

[68] W. G. Hoover, Phys. Rev. A **31**, 1695 (1985).

[69] S. W. Hockney and J. W. Eastwood, *Computer Simulation Using Particles* (CRC Press, Boca Raton, Florida, 1988).

[70] A. K. Rappe, C. J. Casewit, K. S. Colwell, W. A. Goddard III, and W. M. Skiff, J. Am. Chem. Soc. **114**, 10024 (1992).

[71] D. Wolf, P. Keblinski, S. R. Phillpot, and J. Eggebrecht, J. Chem. Phys. **110**, 8254 (1999).

[72] A. M. N. Niklasson, Phys. Rev. Lett. **100**, 123004 (2008).

[73] N. Mathew, M. P. Kroonblawd, T. Sewell, and D. L. Thompson, Mol. Simul. **44**, 613 (2018).

[74] B. Aradi, B. Hourahine, and T. Frauenheim, J. Phys. Chem. A **111**, 5678 (2007), DFTB+ is available at https://www.dftb-plus.info/.

[75] A. A. Hagberg, D. A. Schult, and P. J. Swart, in *Proceedings of the 7th Python in Science Conference*, edited by G. Varoquaux, T. Vaught, and J. Millman (Pasadena, CA, USA, 2008), p. 11, NETWORKX is available at https://networkx.github.io/.

[76] M. Riad Manaa, Appl. Phys. Lett. **83**, 1352 (2003).

[77] M. M. Kuklja and S. N. Rashkeev, Appl. Phys. Lett. **90**, 151913 (2007).

[78] M. P. Kroonblawd, F. Pietrucci, A. M. Saitta, and N. Goldman, J. Chem. Theory Comput. **14**, 2207 (2018).

[79] M. P. Kroonblawd, N. Goldman, and J. P. Lewicki, J. Phys. Chem. B **122**, 12201 (2018).

[80] C. Law and C. J. Sung, Prog. Energy Combust. Sci. **26**, 459 (2000).

[81] M. W. Beckstead, K. Puduppakkam, P. Thakre, and V. Yang, Prog. Energy Combust. Sci. **33**, 497 (2007).

[82] S. Bastea and L. E. Fried, Chemical equilibrium detonation, in *Shock Wave Science and Technology Reference Library: Vol. 6. Detonation Dynamics*, edited by F. Zhang (Springer-Verlag, Berlin Heidelburg, 2012), Chap. 1.

[83] L. E. Fried, in *16th Int. Detonation Symposium* (Office of Naval Research, Arlington, VA, 2018).